Journal of Electrostatics 112 (2021) 103601

Contents lists available at ScienceDirect

Journal of Electrostatics

journal homepage: www.elsevier.com/locate/elstat

Electric force between a dielectric sphere and a dielectric plane

Alberto T. Pérez *, Raúl Fernández-Mateo[1]

Departamento de Electrónica y Electromagnetismo, Facultad de Física, Universidad de Sevilla, Avda. Reina Mercedes s/n, 41012, Sevilla, Spain

A B S T R A C T

We compute the electric force between a dielectric sphere and a dielectric plane in the presence of an external electric field. Laplace's equation is solved in bispherical coordinates and Maxwell's stress tensor is used to calculate the force. The result is given as a series expansion that is evaluated numerically. Asymptotic expressions for the case of large and small distances are obtained and compared with well-known analytical solutions. We use COMSOL commercial software to validate the semi-analytical results.

1. Introduction

The computation of the electric force between particles is a matter of interest in many areas. A non-comprehensive list of these areas is: colloidal suspension [1], electrokinetics [2], powder technology [3], electrostatic precipitators [4], drop manipulation [5], chemical engineering [6], etc. For example, the electrostatic force between colloidal particles may determine their collective behavior [7].

Recently, we have proposed the use of an electric field to control the dynamics of the so-called walking-droplets [8]: under certain conditions, a liquid droplet bouncing over a surface of the same fluid subjected to a vertical oscillation executes an horizontal displacement propelled by the waves its bounces have produced. A good estimation of the electric force is needed to better understand and predict the effects of the application of such electric field to this system.

The electric force between charged and/or conducting particles has attracted special attention, and is the object of many studies [9,10]. Also, the interaction between a charged particle and an external field has been analyzed [11].

Davis [9] used bispherical coordinates to solve the case of two conducing spheres of different sizes in an external field. The case of dielectric particles has also been considered. Nakajima and Sato computed the force between two charged dielectric spheres [12]. Khachatourian et al. [13] computed the force between a charged dielectric sphere and a planar dielectric surface. They made use of bispherical coordinates and a direct integration of the Coulomb force. Keh and Chen also used bispherical coordinates to obtain the electrophoretic mobility of a particle close to a dielectric wall [14].

Love [15] used bispherical coordinates to compute the electric field due to two equal dielectric spheres or a single dielectric sphere and a plane, when an external electric field is applied. In his paper, Love did not compute the electric force between the spheres and the sphere and the plane. In a subsequent paper [16] he applied the same mathematical formalism to obtain the van der Waals forces between two spheres and a sphere and a plane.

The electric potential and field between two different spheres was calculated by Chaumet and Dufour using bispherical coordinates and following the same procedure as Love [17]. Munirov and Filippov obtained the force between two charged dielectric spheres using bispherical coordinates and integrating Maxwell's stress tensor [18].

In this work we compute the electric force between a dielectric sphere and a plane subjected to an external electric field perpendicular to the plane. In order to obtain the electric field we have followed the procedure used by Love. For completeness we recall in Section 3 this procedure. Then, we integrate Maxwell's stress tensor to calculate the force, a procedure similar to the one used by Munirov and Filippov. This is described in Section 4. The limits of small and large distances between the sphere and the plane are analyzed in Section 5. The influence of the dielectric constant of the materials is the subject of Section 6. We have also solved the problem using COMSOL, a commercial software that implements the finite element method. The comparison between both approaches is reported in Section 7.

2. Position of the problem

We consider a dielectric sphere of electric permittivity ε_1 of radius R whose center is at a distance h from a plane. The plane separates the vacuum from another dielectric of permittivity ε_2 which fills the half-space (see Fig. 1). An external electric field E_0 is applied such that, far from the sphere, the field is uniform and perpendicular to the plane.

* Corresponding author.
E-mail address: alberto@us.es (A.T. Pérez).
[1] Also at School of Electronics and Computer Science, University of Southampton, United Kingdom.

https://doi.org/10.1016/j.elstat.2021.103601
Received 11 March 2021; Received in revised form 24 May 2021; Accepted 1 June 2021
Available online 10 June 2021

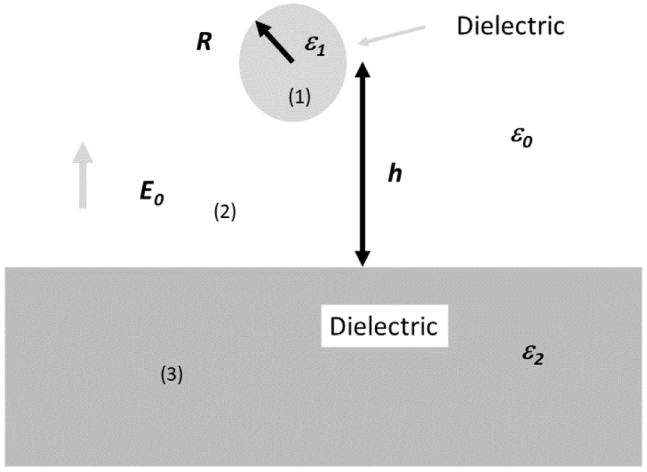

Fig. 1. Geometrical configuration of the problem showing the droplet of radius R, the dielectric bulk and the separation between the center of the droplet and the surface h. The numbers label the different regions.

We will make use of bispherical coordinates (η, τ, ϕ)[15,19]. They are related to the cylindrical coordinates (ρ, z, ϕ) by the equations:

$$z = \frac{d \sinh \eta}{\cosh \eta - \cos \tau}, \quad \rho = \frac{d \sin \tau}{\cosh \eta - \cos \tau} \tag{1}$$

being the azimuthal coordinate ϕ common to both systems.

The η-constant surfaces are spheres of radius $d/\sinh \eta$ centered at $z = \pm \tanh \eta$. The surfaces τ-constant are tori (see Fig. 2). The dielectric sphere corresponds to $\eta = \eta_0 = \cosh^{-1}(h/R)$. The parameter d is given by $d = \sqrt{h^2 - R^2}$. The scale factors are:

$$h_\eta = h_\tau = \frac{d}{\cosh \eta - \cos \tau} \tag{2}$$

3. Solution by separable coordinates

The electric potential Φ is solution of Laplace's equation. Laplace's equation is separable in bispherical coordinates and its solution is found as a series expansion in Legendre's polynomials. We introduce different coefficients for every spatial region [15,19]:

$$\eta_0 \le \eta \quad -\Phi^{(1)} = (\cosh \eta - \cos \tau)^{(1/2)} \sum_{n=0}^{\infty} A_n e^{-(n+1/2)\eta} P_n(\cos \tau) \tag{3}$$

$$0 \le \eta < \eta_0 \quad -\Phi^{(2)} = E_0 z + (\cosh \eta - \cos \tau)^{(1/2)} \times \sum_{n=0}^{\infty} (B_n e^{-(n+1/2)\eta} + C_n e^{(n+1/2)\eta}) P_n(\cos \tau) \tag{4}$$

$$\eta < 0 \quad -\Phi^{(3)} = \frac{\varepsilon_0 E_0 z}{\varepsilon_2} + (\cosh \eta - \cos \tau)^{(1/2)} \times \sum_{n=0}^{\infty} D_n e^{(n+1/2)\eta} P_n(\cos \tau) \tag{5}$$

Region (1) ($\eta_0 \le \eta$) refers to the sphere (with permittivity ε_1), region (2) is the vacuum region ($0 \le \eta \le \eta_0$), and region (3) ($\eta < 0$) refers to the half-space below the plane (with permittivity ε_2). In these expressions we have introduced the electric potential at infinity in the vacuum ($-E_0 z$) and in the dielectric (region 3) ($\varepsilon_0 E_0 z/\varepsilon_2$). In order to apply the orthogonality properties we need to expand z in Legendre's polynomials. The generating function for Legendre polynomials is [19]:

$$\frac{1}{\sqrt{1 + t^2 - 2t \cos \tau}} = \sum_{n=0}^{\infty} t^n P_n(\cos \tau) \tag{6}$$

Introducing $t = e^{-\eta}$:

$$\frac{1}{\sqrt{\cosh \eta - \cos \tau}} = \sqrt{2} \sum_{n=0}^{\infty} e^{-(n+1/2)\eta} P_n(\cos \tau) \tag{7}$$

and taking the derivative, we obtain:

$$z = \frac{d \sinh \eta}{\sqrt{\cosh \eta - \cos \tau}} = \sqrt{2} d (\cosh \eta - \cos \tau)^{(1/2)} \sum_{n=0}^{\infty} (2n+1) e^{-(n+1/2)\eta} P_n(\cos \tau) \tag{8}$$

This expansion is to be included in Eqs. (4)–(5).

3.1. Boundary conditions

The coefficients A_n, B_n, C_n, and D_n in (4) are determined by the corresponding boundary conditions. These are the continuity of the electric potential at every interface:

$$\Phi^{(1)}(\eta = \eta_0) = \Phi^{(2)}(\eta = \eta_0) \tag{9}$$

$$\Phi^{(2)}(\eta = 0) = \Phi^{(3)}(\eta = 0) \tag{10}$$

and the continuity of the normal component of the displacement vector:

$$\varepsilon_1 \left. \frac{\partial \Phi^{(1)}}{\partial \eta} \right|_{\eta=\eta_0} = \varepsilon_0 \left. \frac{\partial \Phi^{(2)}}{\partial \eta} \right|_{\eta=\eta_0} \tag{11}$$

$$\varepsilon_0 \left. \frac{\partial \Phi^{(2)}}{\partial \eta} \right|_{\eta=0} = \varepsilon_2 \left. \frac{\partial \Phi^{(3)}}{\partial \eta} \right|_{\eta=0} \tag{12}$$

The application of three of them is straightforward:

Continuity of the electric potential at the surface of the sphere

$$\eta = \eta_0 \quad A_n = B_n + C_n e^{(2n+1)\eta_0} + \sqrt{2}(2n+1) E_0 d \tag{13}$$

Continuity of the electric potential at the plane

$$\eta = 0 \quad D_n = B_n + C_n \tag{14}$$

Continuity of the normal component of the displacement vector at the plane

$$\eta = 0 \quad \varepsilon_2 D_n = \varepsilon_0 (-B_n + C_n) \tag{15}$$

These three conditions allow us to express the four coefficients in terms of one of them, let us use C_n:

$$A_n = C_n (e^{(2n+1)\eta_0} - \Delta_2) + \sqrt{2}(2n+1) E_0 d \tag{16}$$

$$B_n = -\Delta_2 C_n \tag{17}$$

$$D_n = (1 - \Delta_2) C_n \tag{18}$$

where we have defined:

$$\Delta_1 = \frac{\varepsilon_1 - \varepsilon_0}{\varepsilon_1 + \varepsilon_0}, \quad \Delta_2 = \frac{\varepsilon_2 - \varepsilon_0}{\varepsilon_2 + \varepsilon_0}. \tag{19}$$

The continuity of the normal component of the displacement vector at the sphere surface is more demanding. After some algebra we obtain:

$$\begin{aligned} &\varepsilon_1 \sum_{n=0}^{\infty} A_n e^{-(n+1/2)\eta_0} \left[\sinh \eta_0 - (2n+1)(\cosh \eta_0 - \cos \tau) \right] P_n(\cos \tau) = \\ &\varepsilon_0 \sum_{n=0}^{\infty} \left[B_n e^{(n+1/2)\eta_0} + C_n e^{-(n+1/2)\eta_0} \right] \sinh \eta_0 P_n(\cos \tau) \\ &+ (2n+1)\varepsilon_0 \sum_{n=0}^{\infty} \left[B_n e^{(n+1/2)\eta_0} - C_n e^{-(n+1/2)\eta_0} \right] (\cosh \eta_0 - \cos \tau) \times \\ &P_n(\cos \tau) + \varepsilon_0 \sum_{n=0}^{\infty} E_0 \sqrt{2} d (2n+1) \times \\ &\left[(-\sinh \eta_0 + (2n+1)(\cosh \eta_0 - \cos \tau)) e^{-(n+1/2)\eta_0} \right] P_n(\cos \tau) \end{aligned} \tag{20}$$

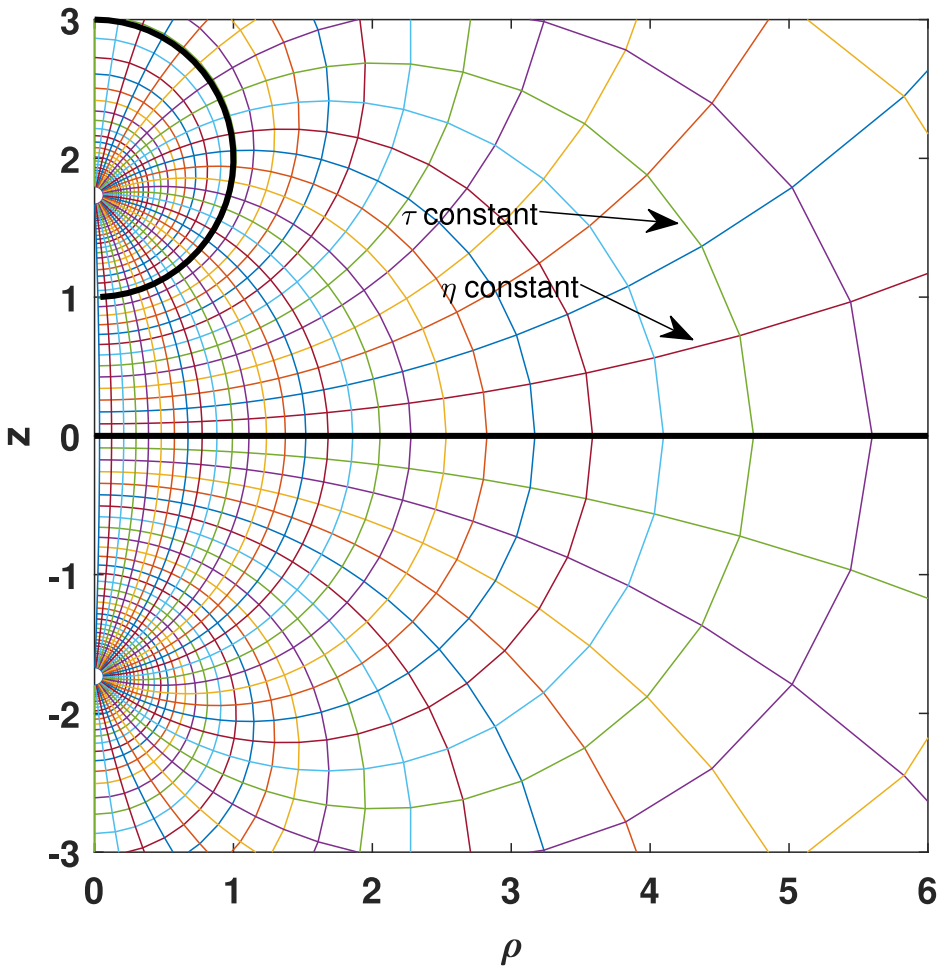

Fig. 2. Section of η and τ coordinate surfaces. For our purposes, the fluid surface corresponds to the $\eta = 0$ coordinate surface and the sphere enclosed in the $\eta = \eta_0 = \cosh^{-1}(h/R)$ surface.

Multiplying by $P_m(\tau)$, taking into account the integrals:

$$\int_{-1}^{1} P_n(x)^2\, dx = \frac{2}{2n+1} \tag{21}$$

$$\int_{-1}^{1} x P_n(x) P_m(x)\, dx = \frac{2n}{4n^2-1}\delta_{n-1,m} + \frac{2(n+1)}{(2n+1)(2n+3)}\delta_{n+1,m} \tag{22}$$

and using (16)–(18), this boundary condition produces a coupling between C_n, C_{n+1} and C_{n-1} that results in the following difference equation:

$$\alpha_n C_{n-1} - \beta_n C_n + \gamma_n C_{n+1} = \lambda_n \quad n = 0, 1, \ldots \tag{23}$$

with

$$\alpha_n = n(e^{-\eta_0} - \Delta_1 \Delta_2 e^{-2n\eta_0}) \tag{24}$$

$$\beta_n = (2n+1)\cosh\eta_0 - \Delta_1 \sinh\eta_0 - \Delta_1 \Delta_2 e^{-2n\eta_0}(n + (n+1)e^{-2\eta_0}) \tag{25}$$

$$\gamma_n = (n+1)(e^{\eta_0} - \Delta_1 \Delta_2 e^{-2(n+1)\eta_0}) \tag{26}$$

$$\lambda_n = 2^{3/2} E_0 d \Delta_1 (n - (n+1)e^{-2\eta_0}) e^{-2n\eta_0} \tag{27}$$

Eq. (23) is a linear inhomogeneous second order difference equation with variable coefficients. It can be solved by a method described by Milne-Thomson [20] and outlined by Love [15]. Following this method we have developed a Matlab script to efficiently solve this equation.

Fig. 3 is a plot of the equipotential lines so-obtained for a typical configuration.

4. Integration of Maxwell's stress tensor

In order to compute the electric force between the sphere and the plane, we integrate Maxwell's stress tensor $\bar{\bar{T}}$ on a surface surrounding the sphere. For convenience, we use the plane $z = 0$ (on the vacuum side) and a semi-sphere of infinite radius (see Fig. 4).

The electric field is given by:

$$\mathbf{E} = -\frac{\cosh\eta - \cos\tau}{d}\left(\frac{\partial \Phi}{\partial \eta}, \frac{\partial \Phi}{\partial \tau}, \frac{1}{\sin\tau}\frac{\partial \Phi}{\partial \phi}\right) \tag{28}$$

and it can be thought as composed by two contributions: the external electric field E_0 and the electric field due to the polarization charges induced on the dielectric surfaces. The last one goes to zero at infinity and its contribution to the integral on the semi-sphere is zero. In the absence of any sphere the force is zero, and the integral of Maxwell's tensor should be zero, that is:

$$\int_{\text{plane}} \bar{\bar{T}}_0 \cdot d\mathbf{a} + \int_{\text{semi-sphere}} \bar{\bar{T}}_0 \cdot d\mathbf{a} = 0 \tag{29}$$

where $\bar{\bar{T}}_0$ is Maxwell's tensor for the electric field E_0 alone.

The force on the sphere is:

$$\mathbf{F} = \int_{\text{plane}} \bar{\bar{T}} \cdot d\mathbf{a} + \int_{\text{semi-sphere}} \bar{\bar{T}} \cdot d\mathbf{a} = \int_{\text{plane}} \bar{\bar{T}} \cdot d\mathbf{a} + \int_{\text{semi-sphere}} \bar{\bar{T}}_0 \cdot d\mathbf{a} \tag{30}$$

since the perturbation due to the sphere does not contribute to the integral over the semi-sphere. Making use of (29), we can restrict the

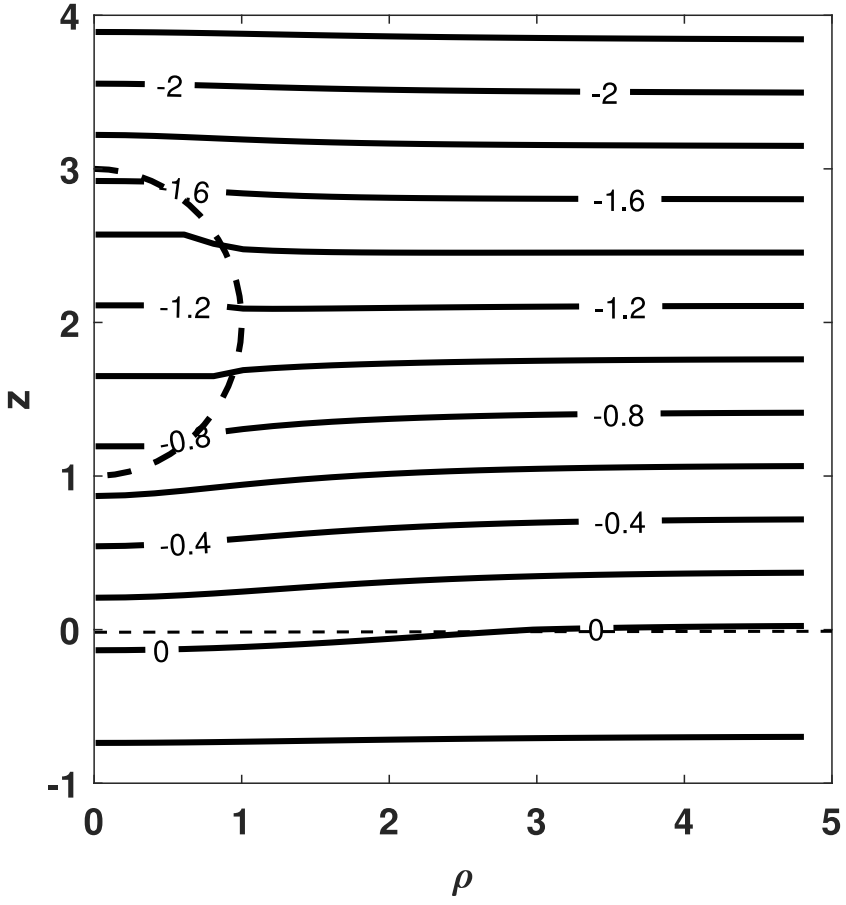

Fig. 3. Contour plot of the electric potential for $\varepsilon_1 = \varepsilon_2 = 2\varepsilon_0$. Numbers indicate the non-dimensional potential.

integration to the plane $z = 0(\eta = 0)$.

$$\mathbf{F} = \int_{\text{plane}} \bar{\bar{T}} \cdot d\mathbf{a} - \int_{\text{plane}} \bar{\bar{T}}_0 \cdot d\mathbf{a} \tag{31}$$

For symmetry reasons, the force has only z-component. Therefore, at the plane $z = 0$ ($\eta = 0$):

$$F_z = \int_{\text{plane}} \left[\frac{1}{2}\varepsilon_0(E_\eta^2 - E_\tau^2) - \frac{1}{2}\varepsilon_0 E_0^2\right] da \tag{32}$$

Using (4) after some algebra, one obtains:

$$\begin{aligned}\frac{dF}{ds} = \frac{1}{2}\varepsilon_0 \Bigg(& 2E_0 \frac{(1-\cos\tau)^{3/2}}{d} \sum_{n=0}^{\infty}(n+1/2)(1+\Delta_2)C_n P_n(\cos\tau) + \\ & + \frac{(1-\cos\tau)^3}{d^2}\left[\sum_{n=0}^{\infty}(n+1/2)(1+\Delta_2)C_n P_n(\cos\tau)\right]^2 - \\ & - \left[\frac{\sin\tau}{2d}(1-\cos\tau)^{1/2}\sum_{n=0}^{\infty}(1-\Delta_2)C_n P_n(\cos\tau) - \right. \\ & \left. - \frac{\sin\tau}{d}(1-\cos\tau)^{3/2}\sum_{n=0}^{\infty}(1-\Delta_2)C_n P_n'(\cos\tau)\right]^2\Bigg)\end{aligned} \tag{33}$$

and

$$F = \int \frac{dF}{ds} h_\tau h_\phi \, d\tau \, d\phi = 2\pi d^2 \int_0^\pi \frac{dF}{ds}\frac{\sin\tau}{(1-\cos\tau)^2} d\tau \tag{34}$$

This integral is a function of the coefficients C_n only and it is ready to be evaluated numerically, and it has been implemented in a Matlab script for that purpose.

We have checked that these expressions in the case $\Delta \to 1$ (conducting limit) produce the same values obtained by Davis [9] for two equal spheres, which is equivalent to one sphere and a plane. The results are also identical to those obtained by Pérez [11] in the case of an uncharged sphere and a plane.

5. Asymptotic behaviors

When the sphere is far from the plane, as compared to its radius, the parameter η_0 is much greater than 1:

$$h \gg R \implies \frac{h}{R} = \cosh\eta_0 \to \frac{e^{\eta_0}}{2} \gg 1 \tag{35}$$

Looking at Eqs. (24)–(27) we see that:

$$\alpha_n \sim n e^{-\eta_0} \tag{36}$$

$$\beta_n \sim e^{\eta_0} \tag{37}$$

$$\gamma_n \sim e^{\eta_0} \tag{38}$$

Regarding parameters λ_n, λ_0 and λ_1 are of the same order of magnitude, and much greater than λ_n for $n = 2, 3, \ldots$. Therefore, the only relevant equations in (23) are:

$$-\beta_0 C_0 + \gamma_0 C_1 = \lambda_0 \tag{39}$$

$$\alpha_1 C_0 - \beta_1 C_1 = \lambda_1 \tag{40}$$

The solution of these equations, to leading order in $e^{-\eta_0}$, is:

$$C_0 = \frac{2}{3-\Delta_1} 2^{3/2} E_0 d \Delta_1 e^{-3\eta_0} \tag{41}$$

$$C_1 = -C_0 \tag{42}$$

Introducing these values in the expression of the force and taking into account that in this limit $e^{-\eta_0} = \frac{R}{2h}$, one obtains:

$$F = 6\pi\varepsilon_0 E_0^2 \frac{\Delta_2 \Delta_1^2}{(3-\Delta_1)^2}\frac{R^6}{h^4} \tag{43}$$

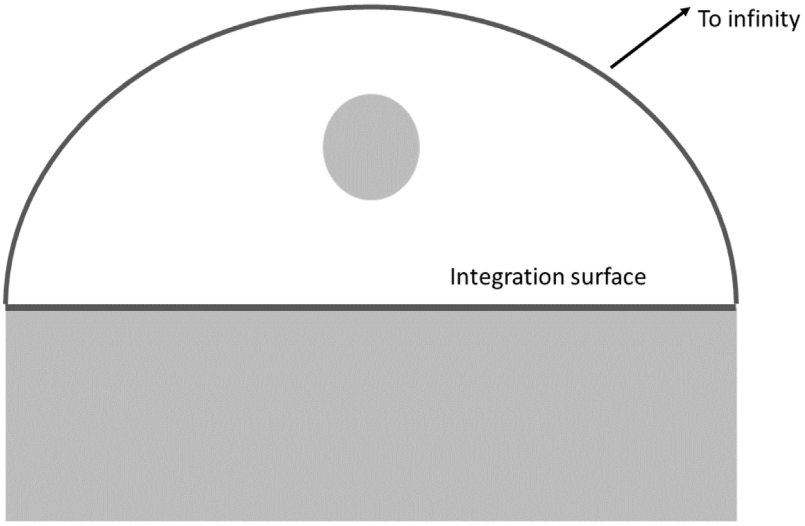

Fig. 4. Integration surface for the computation of the force.

This expression agrees with the one obtained by Lekner [10] for two equal conducting spheres, which is equivalent to a conducting sphere and a plane.

5.1. Comparison with known solutions

The asymptotic value (43) can be compared with two well known solutions: a conducting sphere versus a conducting plane, and a dielectric sphere in front of a conducting plane, both cases in the limit of $h \gg R$.

A conducting sphere in a homogeneous electric field E_0 acquires an electric dipole of value [21]:

$$p = 4\pi\varepsilon_0 R^3 E_0 \tag{44}$$

Therefore, for $h \gg R$ we can neglect the extension of the sphere and consider it as a point dipole. This dipole induces an image dipole on the conductor of the same magnitude and orientation at a distance h from the surface. The force between both dipoles is:

$$F = \frac{6p^2}{4\pi\varepsilon_0 r^4} \tag{45}$$

Since the image dipole is at $r = 2h$:

$$F = \frac{6\pi}{4}\varepsilon_0 E_0^2 \frac{R^6}{h^4} \tag{46}$$

This the limit of expression (43) for $\Delta_1 = \Delta_2 \to 1$

In the case of a dielectric sphere the induced dipole is [21]:

$$p = 4\pi\varepsilon_0 \frac{\varepsilon_1 - \varepsilon_0}{\varepsilon_1 + 2\varepsilon_0} R^3 E_0 \tag{47}$$

The force is:

$$F = \frac{6\pi}{4}\varepsilon_0 \left(\frac{\varepsilon_1 - \varepsilon_0}{\varepsilon_1 + 2\varepsilon_0}\right)^2 E_0^2 \frac{R^6}{h^4} \tag{48}$$

This the limit of expression (43) for $\Delta_2 \to 1$.

Fig. 5 is a plot of the force computed from Eq. (34) as a function of distance for $\varepsilon_2 = \varepsilon_1 = 2.68\varepsilon_0$. The force is presented in non-dimensional form, using $\varepsilon_0 E_0^2 R^2$ as the reference force. Distances are also non-dimensional, being R the scale for distances.

The asymptotic expressions (48) and (49) are also plotted (solid lines). The agreement in the two limits is satisfactory.

5.2. Asymptotic behavior for $h - R \ll R$

When the sphere is very close to the plane its curvature can be neglected. The electric pressure is approximately uniform and of order $\varepsilon_0 E_0^2$. The resulting force may be estimated as this pressure times a contact area proportional to R^2. The result is:

$$F = A\varepsilon_0 E_0^2 R^2 \tag{49}$$

where A is a constant that depends on the dielectric constants. Fig. 5 confirms this estimation.

6. Dependency on the dielectric constant

Fig. 6 is a plot of the computed force as a function of the dielectric constant for a given distance (we chose $h - R = 0.01R$). The force is an increasing function of ε_r, which is taken to be the same for the sphere and the lower half space. For $\varepsilon_r \to 1$ the force vanishes, as it is expected since in that case no polarization charges exist. On the other hand the force tends to saturate for $\varepsilon_r \to \infty$, the conducting limit.

The behavior of the force as a function of the distance as the sphere approaches the plane changes with the dielectric constant (see Fig. 7). In the conducting limit (for $\varepsilon_r \gg 1$) the forces clearly diverges as the distance goes to zero. This is consistent with the results obtained in other works [9–11]. A potential fit gives $F \sim ((h - R)/R)^m$, with $m = -0.8$.

However, as we have shown in the previous section, the force is almost constant for $\varepsilon_r = 2.68$, although looking in detail at the curve a very small increment is observed when the distance decreases (a potential fit gives an exponent $m = -0.02$).

As a general observation one can say that $F \sim ((h - R)/R)^m$, with $m < 0$, for h close to R. The exponent m approaches 0 for $\varepsilon_r \to 1$ and -1 for $\varepsilon_r \to \infty$, taking intermediate values for other values of ε_r. For example, for $\varepsilon_r = 40$ the best fit gives $F \sim ((h - R)/R)^{-0.3}$. But we must say that this potential fit works better for high values of ε_r. For example, for $\varepsilon_r = 2.68$ a linear fit, resulting in no divergency, works better than the potential one. The actual functional dependence must be more complicated than a linear or a potential one, in the line of the type of expression found by Lekner for the conducting case [10].

If the sphere and the plane are made of different materials we have an additional parameter, and things become more cumbersome. In any case, the numerical evaluation of the integral (34) does not present special difficulties. As an example, the force in the case $\varepsilon_1 = 2\varepsilon_0$, $\varepsilon_2 = 4\varepsilon_0$ follows a linear dependence on the distance for close approach: $F/(\varepsilon_0 E_0^2 R^2) = 0.221 - 1.161(h - R)/R$, which gives a finite value when the sphere touches the plane.

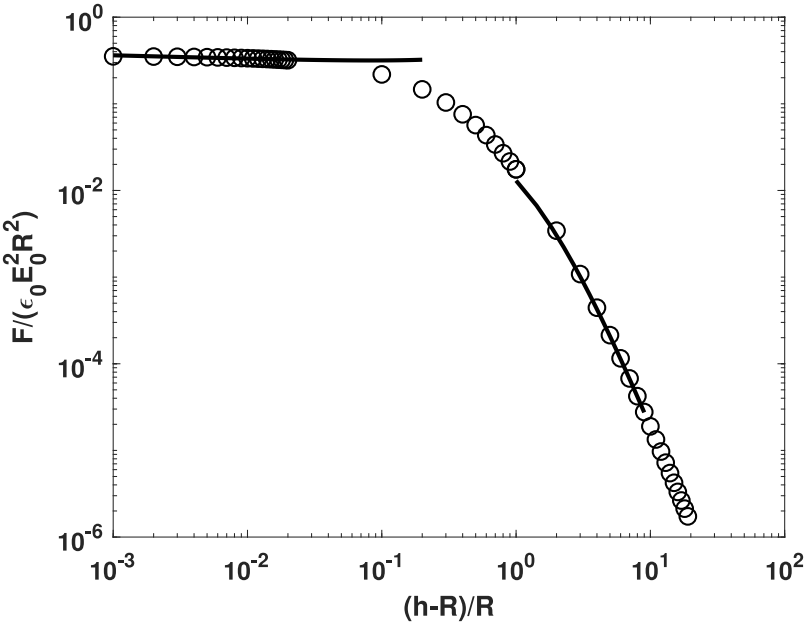

Fig. 5. Computed force as a function of distance. The force is non-dimensionalized with $\epsilon_0 E_0^2 R^2$ and the distance with R. ($\epsilon_2 = \epsilon_1 = 2.68\epsilon_0$). The solid lines represent the asymptotic behavior for small and large distances.

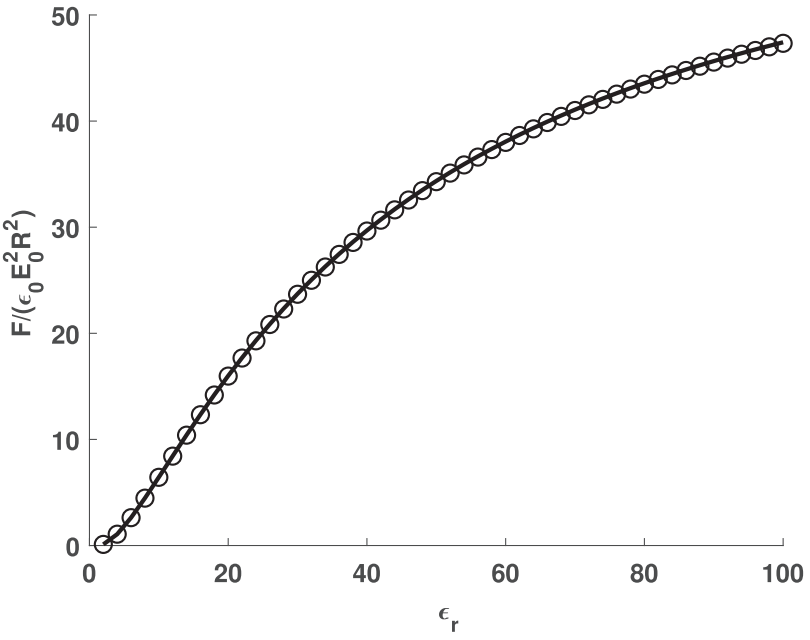

Fig. 6. Computed force as a function of the dielectric constant. The force is non-dimensionalized with $\epsilon_0 E_0^2 R^2$. The non dimensional distance between the sphere and the plane is $(h - R)/R = 0.01$. The solid line corresponds to Eq. (34). The circles are the result of COMSOL finite element method (see below).

7. Comparison with COMSOL numerical solution

7.1. Definition of the domain and boundary conditions

In order to verify and compare the analytical solutions found in the previous sections, we have implemented the equations and boundary conditions described in COMSOL finite element method.

For this purpose, we will use the axial symmetry of the problem to run 2-dimensional simulations reproducing the 3D results needed. This will improve the accuracy of the problem while reducing its computational cost because of the number of mesh nodes the 2D geometry requires with respect to the 3D one.

Therefore, the integral we need to evaluate to compare the simulations with the analytical estimations, represented in Eq. (32), turns into

$$F_z = \int_{\phi=0}^{2\pi} d\phi \int_{\rho=0}^{R_D} \rho d\rho \left[\frac{1}{2}\epsilon_0 (E_z^2 - E_\rho^2) - \frac{1}{2}\epsilon_0 E_0^2\right], \tag{50}$$

where E_z and E_ρ are functions only dependent on the radial and vertical variables.

With this in mind, the resulting geometry, bulk equations and boundary conditions are as represented in Fig. 8. That is, we are imposing the conditions of unperturbed field $\mathrm{E} = E_0\hat{z}$ in the outer boundaries of the domain.

In order to do so, we have to make an estimation of the domain height H_D and width R_D (see Fig. 8) so that the perturbed field

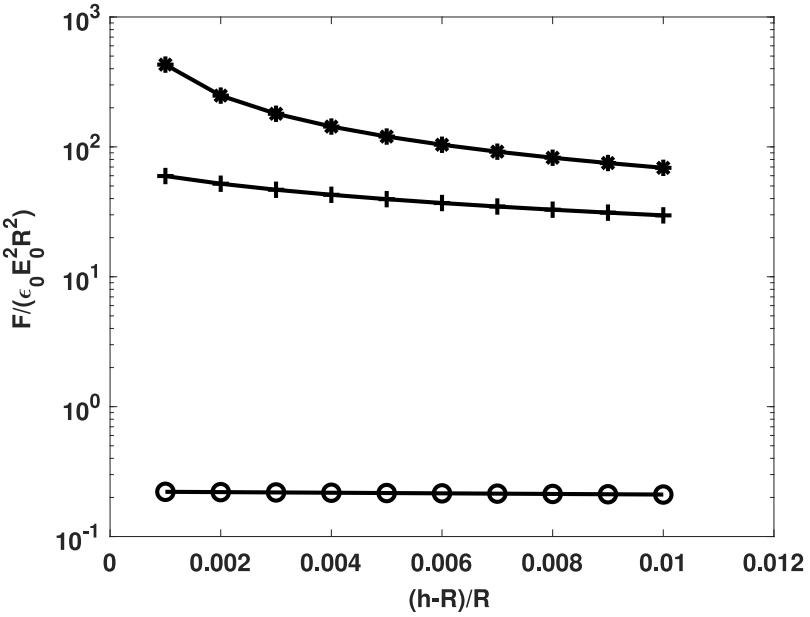

Fig. 7. Computed force as a function of distance for three dielectric constants. The force is non-dimensionalized with $\varepsilon_0 E_0^2 R^2$. The symbols are: $\varepsilon_r = 2\times10^6$ (conducting case) (*); $\varepsilon_r = 40$ (+); $\varepsilon_r = 2.68$ (o).

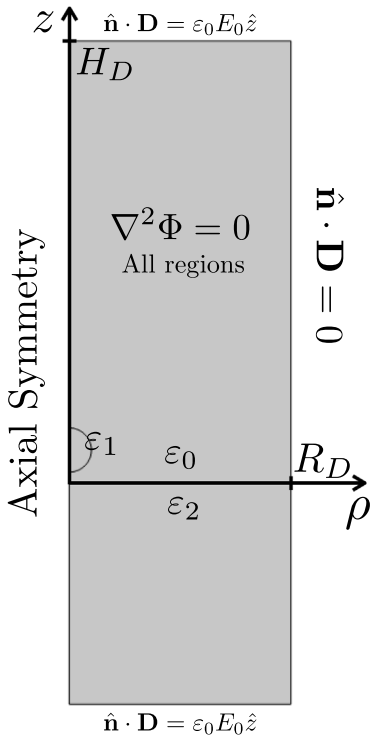

Fig. 8. Domain, bulk equations and boundary conditions imposed in the simulations.

generated by the sphere does not make any significant contribution with respect to the field in absence of sphere, which will ultimately allow us to make use of Eq. (31).

Far from the sphere, if $H_D \gg h$, the sphere may be described as point dipole, as described in Section 5, so the magnitude of the field created by the sphere right above it is given by

$$E = \frac{1}{4\pi\varepsilon_0}\frac{2p}{(H_D-h)^3},$$

which allow us to compare with the applied field magnitude E_0, using (47),

$$\frac{E}{E_0} = 2\frac{\varepsilon_1-\varepsilon_0}{\varepsilon_1+2\varepsilon_0}\left(\frac{R}{H_D-h}\right)^3. \tag{51}$$

In Fig. 9(a) is represented the ratio E/E_0 as a function of the separation between the droplet and the top boundary normalized by the particle radius. It can be observed that at 10 times the particle radius, the field generated by the sphere is already three orders of magnitude less than the applied field, so it is taken to be a reasonable limit for H_D.

For the case of the side boundary at $\rho = R_D$, we choose it so that including an extra distance $\Delta\rho$ makes a relative contribution to the computed force which is less than a given amount δ, that is

$$\frac{F(R_D+\Delta\rho)-F(R_D)}{F(R_D)} < \delta. \tag{52}$$

If $\Delta\rho$ is small enough, $F(\rho)$ can be expanded around R_D which allows us to rewrite the above expression as

$$\frac{1}{F(R_D)}\left.\frac{dF}{d\rho}\right|_{\rho=R_D} < \delta. \tag{53}$$

Now, in order to make an estimation of the distance R_D, we suppose again the sphere to be apart from the evaluating point so that the field can be written as the superposition of the field created by the dipole and the applied field. If we define d as the distance from the center of the sphere to the interface between the fluids at the lateral boundary $d = \sqrt{h^2+R_D^2}$, the components of the field at this curve are

$$E_\rho = 3E_0\frac{\varepsilon_1-\varepsilon_0}{\varepsilon_1+2\varepsilon_0}\frac{\rho R^3}{d^4}, \quad E_z = E_0\left[3\frac{\varepsilon_1-\varepsilon_0}{\varepsilon_1+2\varepsilon_0}\frac{R^3(h-d)}{d^4}+1\right], \tag{54}$$

so that using Eq. (32) we will be able to compute such distance R_D for a given δ. In Fig. 9(b) is represented (53) for ten logarithmically spaced heights of the droplet with respect to the interface.

7.2. Results and comparison with analytical solutions

Using the domain dimensions described above for each height configuration, we computed the force performing a surface integration as indicated in (50) for the same ten logarithmically spaced droplet

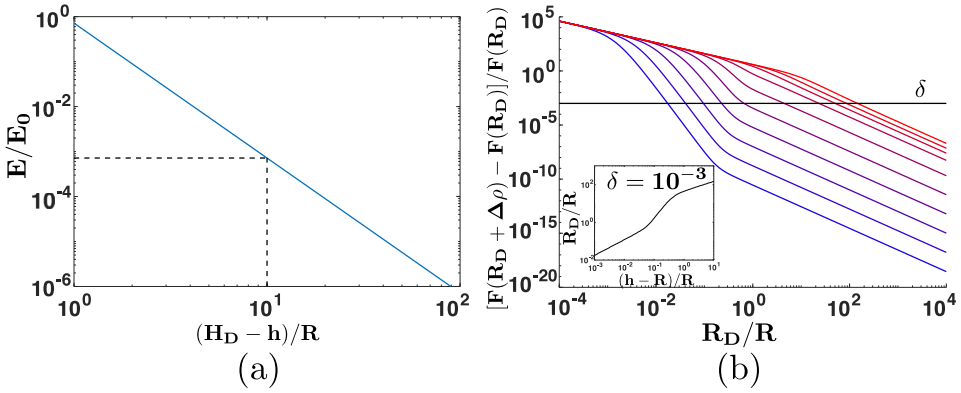

Fig. 9. Choice of boundary limits for the simulations. (a) Upper boundary H_D following equation (51). (b) Lateral boundary R_D using Eq. (53) for ten logarithmically spaced values of h from $(h-R)/R = 10^{-3}$ (bluest curve) to $(h-R)/R = 10$ (reddest curve). In the inner chart it is represented the intersection of the curves with the selected threshold $\delta = 10^{-3}$, which is also given by the horizontal dark line in the main plot. (For interpretation of the references to color in this figure legend, the reader is referred to the web version of this article.)

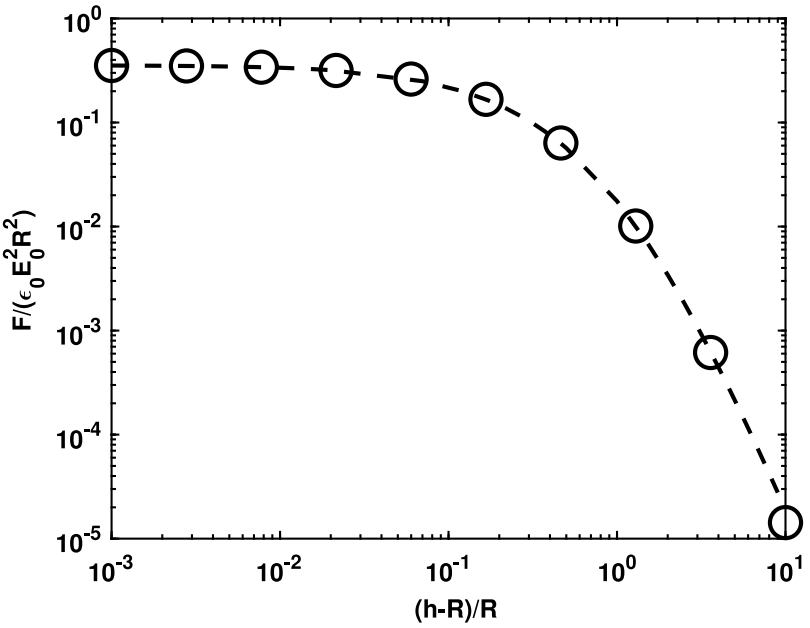

Fig. 10. Force computed from the numerical integration of Eq. (34) (dashed line) in comparison with ten logarithmically spaced configurations simulated with COMSOL following the procedure described in Section 7. As usual, $\epsilon_2 = \epsilon_1 = 2.68\epsilon_0$.

heights represented in Fig. 9(b). These results are presented in Fig. 10. The analytic and numerical values differ in less than 0.06% .

In the same line, Fig. 6 compares the values of the force obtained, with both methods, for a given distance as a function of the dielectric constant. The agreement is, again, very satisfactory.

8. Concluding remarks

In this study we have explored in depth the force between a dielectric sphere and a dielectric plane: we have first set the position of this problem in the literature. Then, we have made a comprehensive study extracting the force from Maxwell's stress tensor and numerically solving the resulting integrals.

We have compared these results with known solutions in two well-known limiting scenarios, serving both as a generalization and a link for them. This is of great interest since many studies that rely on these special circumstances (see for example [8]) would benefit from a deeper understanding in a wider range of separations.

The dielectric constant plays an important role in the magnitude and the spatial dependence of the force. In the conducting limit the force increases without limit when the separation between the sphere and the plane decreases. This is not the case for small dielectric constants.

Finally, we have complemented these calculations with numerical simulations of the system using the finite element method implemented in COMSOL commercial software. This provides a more intuitive view on the study which is also in good agreement with the initial analytic approach.

Declaration of competing interest

The authors declare that they have no known competing financial interests or personal relationships that could have appeared to influence the work reported in this paper.

Data availability

Data sharing is not applicable to this article as no new data were created or analyzed in this study.

Acknowledgments

This work was funded by the Spanish Ministerio de Ciencia, Innovación y Universidades under Research Project No. PGC2018-099217-B-I00, by the Ministerio de Economía y Competitividad, Spain under Research Project No. CTQ2017-83602-C2-2-R, and Junta de Andalucía, Spain under research project 2019/FQM-253.

References

[1] T.B. Jones, T.B. Jones, Electromechanics of Particles, Cambridge University Press, 2005.
[2] N.G. Green, A. Ramos, H. Morgan, Ac electrokinetics: a survey of sub-micrometre particle dynamics, J. Phys. D: Appl. Phys. 33 (6) (2000) 632.
[3] A. Castellanos, The relationship between attractive interparticle forces and bulk behaviour in dry and uncharged fine powders, Adv. Phys. 54 (4) (2005) 263–376.
[4] K. Adamiak, P. Atten, Numerical simulation of the 2-D gas flow modified by the action of charged fine particles in a single-wire ESP, IEEE Trans. Dielectr. Electr. Insul. 16 (3) (2009) 608–614.
[5] J.L. Roux, Y. Fouillet, Forces and charges on an undeformable droplet in the DC field of a plate condenser, J. Electrost. 66 (2008) 283–293.
[6] M.L. Grant, D.A. Saville, Electrostatic interactions between a nonuniformly charged sphere and a charged surface, J. Colloid Interface Sci. 171 (1) (1995) 35–45.
[7] K. Barros, E. Luijten, Dielectric effects in the self-assembly of binary colloidal aggregates, Phys. Rev. Lett. 113 (1) (2014) http://dx.doi.org/10.1103/PhysRevLett.113.017801.
[8] R. Fernández-Mateo, A.T. Pérez, Faraday waves under perpendicular electric field and their application to the walking droplet phenomenon, Phys. Fluids 33 (1) (2021) 017109.
[9] M.H. Davis, Two charged spherical conductors in a uniform electric field: Forces and field strength, Quart. J. Mech. Appl. Math. 17 (4) (1964) 499–511.
[10] J. Lekner, Forces and torque on a pair of uncharged conducting spheres in an external electric field, J. Appl. Phys. 114 (22) (2013) 224902.
[11] A.T. Pérez, Charge and force on a conducting sphere between two parallel electrodes, J. Electrost. 56 (2) (2002) 199–217.
[12] Y. Nakajima, T. Sato, Calculation of electrostatic force between two charged dielectric spheres by the re-expansion method, J. Electrost. 45 (1999) 213–226.
[13] A. Khachatourian, H.-K. Chan, A.J. Stace, E. Bichoutskaia, Electrostatic force between a charged sphere and a planar surface: A general solution for dielectric materials, J. Chem. Phys. 140 (7) (2014) http://dx.doi.org/10.1063/1.4862897.
[14] H.J. Keh, S.B. Chen, Electrophoresis of a colloidal sphere parallel to a dielectric plane, J. Fluid Mech. 194 (1988) 377–390.
[15] J.D. Love, Dielectric sphere-sphere and sphere-plane problems in electrostatics, Q. J. Mech. Appl. Math. 28 (1975) 449–471.
[16] J.D. Love, Vanderwaals force between 2 spheres or a sphere and a wall, J. Chem. Soc.-Faraday Trans. II 73 (1977) 669–688.
[17] P.C. Chaumet, J.P. Dufou, Electric potential and field between two different spheres, J. Electrost. 43 (1998) 145–159.
[18] V.R. Munirov, A.V. Filippov, Interaction of two dielectric macroparticles, J. Exp. Theoret. Phys. 117 (5) (2013) 809–819, http://dx.doi.org/10.1134/S1063776113130050.
[19] P.M. Morse, H. Feshback, Methods of Theoretical Physics, McGraw-Hill, 1953.
[20] L.M. Milne-Thomson, The Calculus of Finite Differences, American Mathematical Soc., 2000.
[21] J.D. Jackson, Classical Electrodynamics, Wiley, 1998.